The partition constant of binary mixtures for the equilibrium between a bulk and a confined phase

Henry A. Cortés,[†,‡] Damian A. Scherlis,[†] and Matías H. Factorovich[*,†]

†*Departamento de Química Inorgánica, Analítica y Química Física/INQUIMAE, Facultad de Ciencias Exactas y Naturales, Universidad de Buenos Aires, Ciudad Universitaria, Pab. II, Buenos Aires (C1428EHA) Argentina.*

‡*BCAM-Basque Center for Applied Mathematics, Alameda de Mazarredo 14, E-48009 Bilbao, Spain*

E-mail: mfactorovich@qi.fcen.uba.ar

Abstract

It is well known that the thermodynamic, kinetic and structural properties of fluids, and in particular of water and its solutions, can be drastically affected in nanospaces. A possible consequence of nanoscale confinement of a solution is the partial segregation of its components. Thereby, confinement in nanoporous materials (NPM) has been proposed as a means for the separation of mixtures. In fact, separation science can take great advantage of NPM due to the tunability of their properties as a function of nanostructure, morphology, pore size, and surface chemistry. Alcohol-water mixtures are in this context among the most relevant systems. However, a quantitative thermodynamic description allowing for the prediction of the segregation capabilities as a function of the material-solution characteristics is missing. In the present study we attempt to fill this vacancy, by contributing a thermodynamic treatment for the calculation of the partition coefficient in confinement. Combining the multi-layer adsorption model for binary mixtures with the Young equation, we conclude that the liquid-vapor surface tension and the contact angle of the pure substances can be used to predict the separation ability of a particular material for a given mixture to a semi-quantitative extent. Moreover, we develop a Kelvin-type equation that relates the partition coefficient to the radius of the pore, the contact angle and the liquid-vapor surface tensions of the constituents. To assess the validity of our thermodynamic formulation, coarse grained molecular dynamics simulations were performed on models of alcohol/water mixtures confined in cylindrical pores. To this end, a coarse-grained amphiphilic molecule was parameterized to be used in conjunction with the mW potential for water. This amphiphilic model reproduces some of the properties of methanol such as enthalpy of vaporization and liquid-vapor surface tension, and the minimum of the excess enthalpy for the aqueous solution. The partition coefficient turns out to be highly dependent on the molar fraction, on the interaction between the components and the confining matrix, and on the radius of the pore. A remarkable agreement between the theory and the simulations is found for pores of radius larger than 15 Å.

I. Introduction

The widespread interest in nanoporous materials (NPM) that is growing across a number of different technological fields[1,2] finds its explanation in the recent advances in the synthetic techniques that allow for a fine tunability of nanostructure, morphology, pore size, and modification of surface chemistry. These characteristics provide control on a variety of physical and chemical properties essential for several applications, such as molecular and ionic sieving,[3,4] gas storage,[5] molecular detection[6] and separation science.[7–9] In the context of the latter application, the thermodynamic partition constant constitutes the key parameter to quantify the separation process. If $\chi_{i;j}$ is the molar fraction of the component i in the phase j and $\gamma_{j;i}$ is the activity coefficient with the same nomenclature, the partition constant K for a mixture of A and B can be defined according to the following relation:[10,11]

$$K = \frac{x_{A;ads} \cdot x_{B;blk}}{x_{A;blk} \cdot x_{B;ads}} \cdot \frac{\gamma_{A;ads} \cdot \gamma_{B;blk}}{\gamma_{A;blk} \cdot \gamma_{B;ads}}. \tag{1}$$

This expression implies the existence of two phases, a liquid or bulk one (blk), and a confined or adsorbed one (ads), which are assumed to be in equilibrium. Between these two phases an exchange process occurs involving the components of the mixture, which can be represented as $A(blk) + B(ads) \rightleftharpoons A(ads) + B(blk)$. The product of the molar fraction (χ) with the activity coefficient (γ) gives the activity of the component i on phase j ($a_{i;j}$). The quotient of the molar fractions (first quotient on the right in Eq. 1) is called the partition coefficient and is usually designated with the letter S. The partition coefficient equals the partition constant (K) when the system behaves ideally, i.e., when the activity coefficients are equal to 1, or when their ratio is 1.

To compute S, all the molar fractions must be known, which requires a consistent definition of $\chi_{i;ads}$. The adsorbed molar fraction is however not unequivocally defined, because it relies on an underlying model of the pore. In experiments, it depends on the model adopted to analyze the adsorption data,[11,12] while in simulations, it can be directly computed pro-

vided that all the solution inside the pore is considered to be the adsorbed phase (this last definition will be the one used during this work).

Among the most relevant systems that could take advantage of NPM-based separation, alcohol-water binary mixtures have received special attention. The importance of alcohols in the chemical industry and the difficulty of separating them from their aqueous solutions, a consequence of their hydrophilic nature, makes these mixtures good candidates for this technique, envisioned as a promising route to replace the conventional distillation method, which is an expensive, inefficient and high energy-consuming.[7,13]

Several types of NPM have shown potential for alcohol-water mixture separation. Hexagonal boron nitride (hBN),[14] metal carbides and nitrides (Mxenes),[15] metal oxide frameworks (MOFs),[16] mesoporous silica,[17] and carbon materials,[18,19] are some of the most relevant. Particularly, carbon materials have gained importance thanks to their low cost of synthesis and their exceptional mechanical properties. In general, the separation ability is namely attributed to the preferential affinity of the surface for one of the species of the mixture and to the size selective penetration through the pore.[7,20,21] However, a rational design of these NPM for the separation of substances requires a thorough understanding of how the mixture concentration, pore size and pore surface functionalization affect the structure and thermodynamic properties of the confined solution. There are still many specific questions regarding the behavior of fluids in confinement, which clarification could provide a quantitative relation between these variables.[13]

As a consequence of the physical complexity, very few works have been able to experimentally address the microsegregation and percolation in confinement.[17,22,23] Resorting to atomic force microscopy measurements, Zandvliet and co-workers[22] studied mixtures of small alcohols and water confined between mica and graphene. They reported evidence of alcohol islands surrounded by a water film and a remarkable reduction of the alcohols diffusion coefficients, dependent on the molecule size. At the same time, based on neutron scattering measurements of the hydrogen-bond forming mixture of terbutanol and toluene, completely

miscible in bulk, Mhanna and collaborators[23] observed the existence of domains exhibiting different compositions when confined in mesoporous silica. Employing a core-shell model, these authors concluded that those domains consist in cylindrical structures with the terbutanol molecules surrounding those of tolueno. More recently, Muthulakshmi and co-authors[17] reported a similar behavior for ethanol–water mixtures confined in mesoporous silica using positron annihilation lifetime spectroscopy. They showed the presence of bulk-like mixtures at the core of the pore and a distinct interfacial phase near the pore wall, which was associated with ethanol molecules anchored at the surface.

Molecular dynamics (MD) simulations, on the other hand, have been of great help in the interpretation of experimental results and in providing a microscopic picture of the structure and the dynamics of mixtures in confinement.[24–33] Specifically for alcohol/water mixtures, they allowed for the characterization of the dehydration of carbon nanotubes immersed in alcohol-water solutions, resulting from a preferential adsorption of alcohols that decreases as the pore diameter increases.[27,28] The selectivity for alcohols has also shown a dependence on molecular length.[28] Furthermore, a layered structure of the mixture is typically observed within nanopores. This behavior appears to be independent of pore shape (cylindrical or slit), with the position of the alcohol layer depending directly on the hydrophobicity of the pore walls.[29–33] Analogously, it was observed a inhibited diffusion for both alcohol and water molecules, stemmed from the structuring induced by confinement. This behavior has, in turn, been associated with a coordinated movement of both components.[29,30,32]

In spite of all these efforts to elucidate the microphase demixing within nanopores, there are still central questions which remain mostly unexplored. One of the central issues in this sense is the dependence of the partition constant with respect to pore radius and surface affinity. This is precisely the question that we address in the present study, where we derive a formal relation between K and such parameters. Molecular dynamics simulations are performed to put this relation to the test for a mixture of water and alcohol .

II. Methodology

Water was described with the coarse-grained model mW,[34] in which each molecule is represented by a single particle interacting through anisotropic short-range forces. This model does not have electrostatic interactions and is based on the short-ranged Stillinger-Weber (SW) potential,[35] which consists of a sum of two-body attraction terms that favor high coordination and three-body repulsion terms that encourage tetrahedral "hydrogen-bonded" configurations.[34] The mW model has been extensively validated for the study of the structure and thermodynamic properties of water in bulk and confinement.[34,36–43]

The amphiphilic molecule (Am) used to represent the alcohol was formed by two subunits, one hydrophilic (OH equal to mW) and the other hydrophobic (M). The interaction between both particles was described through the two-body term on the SW potential with $\lambda = 0$, ϵ_{M-mW} =0.180 kcal/mol and σ_{M-mW} =4.0 Å, and the rest of the parameters set equal to those for mW.[34] The bond parameters were taken from the UA-OPLS force field for the CH_3 group[44] and were kept fixed with the shake algorithm. The interactions between hydrophobic particles were also represented by the two-body term of the SW potential with $A = B$ =1, p =8, q =4, a =1.2, ϵ_{M-M} =0.118 kcal/mol and σ_{M-M} =4.0 Å. Since the hydrophilic group was modeled as a mW particle, the interactions between the hydrophilic group and water was modeled in the mixture in analogy to those between water molecules, a strategy previously used by Molinero and coworkers.[45]

The pores were composed from mW particles, with a structure derived from an instantaneous configuration of liquid mW water simulated at 298 K and 1 atm in periodic boundary conditions, following a protocol established in previous studies.[36,46] Cylindrical nanopores of 100 Å in length and radii between 5 and 30 Å, were built by removing a cylinder of water from the center of the simulated water box. The walls were always wider than 12 Å, well beyond 9.2 Å, the largest cutoff for the simulation. The interaction of mW and M with the wall particles (W) were also described by the two-body terms of the SW potential, setting $\lambda = 0$ and tuning ϵ_{mW-W} to attain different degrees of hydrophobicity for the surface. This

hydrophobicity was characterized in terms of the contact angle (θ), which has been estimated from simulations of droplets on flat surfaces with the same amorphous structure as the pore walls. The methodology, described in detail elsewhere,[36,47] was adapted from the method originally proposed by Giovambattista *et al.*[48] Unless otherwise noticed, we used ϵ_{mW-W} =0.35 kcal/mol, ϵ_{M-W} =0.095 kcal/mol, σ_{mW-W} =3.56 Å, σ_{M-W} =4.0 Å, and the rest of the parameters set equal to those corresponding to mW.[45] These values give contact angles θ_{Am}=36° and θ_{mW} =80° for the pure liquids, in line with experimental reports for methanol and water on different hydrophobic materials,[49,50] representing a mild type of hydrophobicity ($\theta_{mW-W} < 90°$). In section III.E, the role of the surface interaction on the partition coefficient is analyzed, for which purpose we have varied ϵ_{mW-W} over a range from 0.05 to 0.35 kcal/mol, which translates into a contact angle ranging from 80° to 130 °. Such contact angle values are found in several materials such as silica nanopores derivatized with different sylilating agents.[51]

The pore model, of 100 Å length, occupied the center of the simulation box with periodic boundaries. The liquid mixture completely filled the interior of the pore plus a region extending 60 Å, leaving a gas phase of other 60 Å in between the two liquid reservoirs, as shown in Figure 1. These reservoirs act as bulk solutions in contact with the confining matrix. In particular, for the simulation of the most diluted solution, of global composition $\chi^{\circ}_{Am} = 0.1$, the dimension of the liquid reservoir was duplicated on both sizes and the limits of the cell adapted to keep the volume of vacuum.

Molecular dynamics simulations were performed using LAMMPS.[52] The equations of motion were integrated in a canonical (NVT) ensemble with the velocity Verlet algorithm using a time step of 5 fs. Periodic boundary conditions were applied on the three dimensions. The temperature was controlled with the Nosé-Hoover thermostat with a relaxation time of 0.5 ps. The model systems were prepared by filling completely the pore and part of the external region with the molecules randomly distributed, with those in the reservoirs limited by a vacuum region, as shown in Figure 1. The simulations were performed for mixtures

with global molar fractions of Am (χ°_{Am}) varying between 0 and 1 and for pores in a range from 5 to 30 Å radii. In all cases the positions of the particles belonging to the pore walls were fixed. All runs were subject to an equilibration process following the protocol proposed by de la LLave *et al.*[46] Simulations were performed along 200 ns for 5 independent runs, each one with distinct initial velocities. Statistical sampling was done on the last 100 ns.

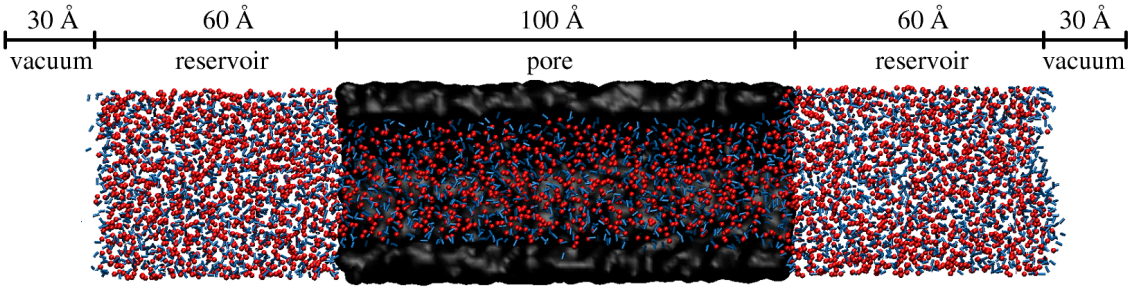

Figure 1: Structure of the pore model including the bulk phase in equilibrium. Snapshot extracted from MD simulations for a mixture of water (red spheres) and Am (blue rods) with a global molar fraction χ°_{Am} =0.5. The nanopore structure is represented as a black surface.

The partition coefficient is computed as the average value resulting from the five replicas, with the error bars computed as confidence intervals at 95% with the formula $\pm t_{0.95;n-1} \cdot std(S)/\sqrt{n}$, where $t_{0.95;n-1}$ is the student t function at 95% of confidence with n-1 degrees of freedom, n is five for this case, and $std(S)$ is the standard deviation associated with the partition coefficient from the five replicas.

III. Results and discussion

III.A Relation between the partition function and surface affinities

Assuming a multi-layer adsorption model,[53] Gritti and co-authors departed from the chemical potential of a component i in the adsorbed and in the bulk liquid phases ($\mu_{i;ads}$ and

$\mu_{i;blk}$),

$$\begin{aligned}\mu_{i;blk}(T,x_i) &= \mu^*_{i;blk}(T) + RT\ln(x_{i;blk}\gamma_{i;blk}),\\ \mu_{i;ads}(T,x_i) &= \mu^*_{i;blk}(T) - \int_{\sigma_i^{*;sl}}^{\sigma_i^{sl}(x_i)} \overline{a}_i d\sigma^{sl} + RT\ln(x_{i;ads}\gamma_{i;ads}),\end{aligned} \tag{2}$$

to relate the partition constant K (Eq. 1) with the molar area ($\overline{a}_i$) and the solid-liquid surface tension (σ^{sl}):

$$RT\ln(K) = \int_{\sigma_A^{*;sl}}^{\sigma^{sl}(x_A)} \overline{a}_A d\sigma_A^{sl} - \int_{\sigma_B^{*;sl}}^{\sigma^{sl}(x_B)} \overline{a}_B d\sigma_B^{sl} \tag{3}$$

where the asterisk (*) refers to the pure liquid. This equation reflects the fact that the equilibrium constant depends on the surface tension which in turn is a function of the composition. An analogy to a bulk system could be the change in the equilibrium constant of a chemical reaction due to an applied external pressure: the equilibrium constant K_c will increase or decrease with the applied pressure depending on the partial molar volumes of the species involved. In the adsorption case, the free energy of the adsorbed molecules is determined by the surface tension. Still, unlike the bulk example, the surface tension depends on the composition in a way that, at variance with the external pressure, can not be independently controlled.

Eq. 3 allows us to rationalize the magnitude of the partition constant as a function of the solid-liquid surface tension (σ^{sl}). Unfortunately the value of σ^{sl} is seldom accessible through experiments or simulations, nevertheless it can be substituted by Young's equation, $\sigma^{sl} = \sigma^{sv} - \sigma^{lv}cos(\theta)$. Then, Eq. 3 can be integrated in combination with Young's equation, assuming that molar areas are constant and that σ^{sv} is an intrinsic property of the solid, independent of the composition of the solution. In that case the results is:

$$RT\ln(K) = \left(\overline{a}^*_A\sigma^{*;lv}_A cos(\theta^*_A) - \overline{a}^*_B\sigma^{*;lv}_B cos(\theta^*_B)\right) - \left(\overline{a}^*_A - \overline{a}^*_B\right)\sigma^{lv}cos(\theta). \tag{4}$$

The product between $cos(\theta)$ and σ^{lv}, equal to the difference between the solid-vapor and

solid-liquid surface tensions, is a measure of the affinity of the species (or of the solution) for the surface. It can be interpreted as the free energy associated with the wetting process.

Two limiting cases are of interest in Eq. 4. When A is at infinite dilution $\sigma^{lv}cos(\theta) \rightarrow \sigma_B^{*;lv}cos(\theta_B^*)$ and therefore

$$\lim_{\chi_A \to 0} RT \ln(K) = \overline{a}_A^*[\sigma_A^{*;lv}cos(\theta_A^*) - \sigma_B^{*;lv}cos(\theta_B^*)] \tag{5}$$

holds. The other limit is when the fraction of B approaches 0, in which case $\sigma^{lv}cos(\theta) \rightarrow \sigma_A^{*;lv}cos(\theta_A^*)$ and the partition coefficient is given by

$$\lim_{\chi_A \to 1} RT \ln(K) = \overline{a}_B^*[\sigma_A^{*;lv}cos(\theta_A^*) - \sigma_B^{*;lv}cos(\theta_B^*)]. \tag{6}$$

This result indicates that a range for the partition constant can be estimated from measurements of the liquid-vapor surface tensions of the pure components and their contact angles with the material of interest. These properties are routinely determined in the laboratory and computed in molecular simulations. Even if the molar areas remain unknown, the difference $\sigma_A^{*;lv}cos(\theta_A^*) - \sigma_B^{*;lv}cos(\theta_B^*)$ can provide a qualitative hint regarding the partition performance of a certain solid for a given solution. The validity of these limiting cases is examined via MD simulations in section III.E

III.B The dependence on pore radius

Equation 3 does not exhibit an explicit dependence of K with respect to pore radius; such a dependence then might be hidden in the molar areas $\overline{a}_i$ (assuming that the surface tension can be considered constant with curvature). To establish a connection between K and the pore radius, in what follows we analyze this phenomenon in terms of the Kelvin equation, which describes the vapor pressure of pure systems exposing curved interfaces and is therefore used for fluids confined in different geometries.[36,54] In particular, the treatment we develop in this section is partially inspired on a work by Shardt and collaborators, who derived and

verified a Kelvin-type equation for confined mixtures with weakly to non-interacting walls.[55]

The vapor-solid adsorption of mixtures can be related to liquid-solid adsorption if the vapor is in equilibrium with both, the fluid mixture in the solid (the confining matrix) and a liquid reservoir (the bulk solution).[56] For this setup, the liquid-solid excess adsorption isotherm has been obtained from vapor-solid adsorption data.[57,58] Here we present a derivation of an expression for the partition coefficient that follows that of the Kelvin equation. We begin by writing the chemical potential of component i of the mixture under confinement,

$$\mu_{i;ads}(T, P_M) = \mu^*_{i;blk}(T, P^\infty_{i;vap}) + \int_{P^\infty_{i;vap}}^{P_M} \overline{V}^*_{i;blk} dp + RT \ln(a_{i;ads}). \tag{7}$$

Here $P^\infty_{i;vap}$ denotes the vapor pressure of the reference planar interface (of infinite curvature) for the pure component i, while P_M refers to the mechanical pressure arising from the confinement of the solution. $\overline{V}^*_{i;blk}$ is the molar volume of the pure liquid i, $a_{i;blk}$ is the activity of component i in the confined solution, and $\mu^*_{i;blk}(T, P^\infty_{i;vap})$ is the reference chemical potential of component i in contact with a planar surface. Upon integration and considering the solution is an incompressible fluid ($\overline{V}^*_{i;blk}$ is constant with respect to pressure), we get:

$$\mu_{i;ads}(T, P_{vap}) = \mu^*_{i;blk}(T, P^\infty_{i;vap}) + (P_M - P^\infty_{i;vap})\overline{V}^*_{i;blk} + RT \ln(a_{i;ads}). \tag{8}$$

Replacing P_M by the Laplace expression for a cylindrical capillary of radius r_p,[54] $P_M - P_{vap} = -2\sigma^{lv} cos(\theta)/r_p$, and assuming $P_{vap} - P^\infty_{i;vap}$ is negligible, we obtain

$$\mu_{i;ads}(T, P_{vap}) = \mu^*_{i;liq}(T, P^\infty_{i;vap}) - \frac{2\sigma^{lv} cos(\theta)}{r_p}\overline{V}^*_{i;blk} + RT \ln(a_{i;ads}). \tag{9}$$

Now a key approximation is introduced: we assume that each component of the mixture interacts with the environment independently from the presence of the other, making σ^{lv} and $cos(\theta)$ equal to the surface tension and contact angle of the pure substances. This approximation is similar to the idea behind the Ideal Adsorbed Solution theory,[59] where the

adsorption isotherm of a mixture can be represented as the combination of those corresponding to the pure components. Hence the expression for the chemical potential can be written as:

$$\mu_{i;ads}(T, P_{vap}) = \mu^*_{i;liq}(T, P^{\infty}_{i;vap}) - \frac{2\sigma^{*;lv}_i cos(\theta^*_i)}{r_p}\overline{V}^*_{i;blk} + RT\ln(a_{i;ads}). \tag{10}$$

In the vapor phase, the chemical potential for component i is simply $\mu_{i;vap}(T, P_{i;vap}) = \mu^{\theta}(T) + RT\ln\left(P_{i;vap}/P^{\theta}\right)$ and for the bulk solution is $\mu_{i;blk}(T, P_{i;vap}) = \mu^*_{i;liq}(T, P^{\infty}_{i;vap}) + RT\ln(a_{i;blk})$. Taking into account that the three portions of the system are in equilibrium, $\mu_{i;blk}(T, P_{i;vap}) = \mu_{i;vap}(T, P_{i;vap}) = \mu_{i;ads}(T, P_{i;vap})$, we can focus on the confined and bulk phases to arrive to the relation

$$RT\ln(\frac{a_{i;blk}}{a_{i;ads}}) = -\frac{2\sigma^*_{i;lv} cos(\theta^*_i)}{r_p}\overline{V}^*_{i;blk}. \tag{11}$$

Since the partition constant is defined as $K = a_{A;ads}a_{B;blk}/a_{A;blk}a_{B;ads}$, equation 11 allows us to write:

$$RT\ln(K) = \frac{2}{r_p}(\sigma^{*;lv}_A cos(\theta^*_A)\overline{V}^*_{A;blk} - \sigma^{*;lv}_B cos(\theta^*_B)\overline{V}^*_{B;blk}) \tag{12}$$

This expression relates the partition coefficient directly with the radius of the pore (r_p) and the difference in the affinities for the solid ($\sigma^{*;lv}_i \cos(\theta^*_i)$). This model is put to the test in section III.E below.

III.C A coarse-grained alcohol model

The bulk density, enthalpy of vaporization, and surface tension of the amphiphilic molecule Am (see parameters in section II) were calculated following the methodology employed by Caleman *et al.*,[60] but with a modification in the way the potential energy of the gas phase is computed. In the present case, we used a small number of molecules, in a simulation box with large enough dimensions, as to render negligible the interactions among them. The

resulting values were ρ=1.11 g/cm^3, ΔH_{vap}=40.91 KJ/mol, and $\sigma^{*,lv}$=23.94 mN/m. The corresponding experimental values for methanol are 0.79 g/cm^3,[61] 37.6 KJ/mol[62] and 22.70 mN/m.[63] The density difference of 40% between the Am model and methanol indicates that our force-field produces a compact structure compared to methanol, but in contrast, ΔH_{vap} and $\sigma^{*;lv}$, with differences of 8% and 5%, reasonably agree with the experimental behavior of this alcohol. Other well-known potentials like the OPLS/AA and GAFF have been reported to give a better match for the density, while resulting in similar deviations for ΔH_{vap} and $\sigma^{*,lv}$.[60]

As we are interested in Am-mW mixtures under confinement, we computed the bulk enthalpy of mixing (ΔH_{mix}) and the liquid-vapor surface tension for the solution. Figure 2 (Left) presents results for ΔH_{mix} versus χ_{Am}, showing a qualitative agreement in terms of the magnitude of ΔH_{mix}. The minimum is displaced around 0.2 units of molar fraction with respect to the experiment, which exhibits its minimun at $\chi_{Am} \approx 0.5$. In turn, ΔH_{mix} at the minimum, of -0.225 Kcal/mol, turns out to be 10% lower than the experimental value. It is important to note that these features are very difficult to reproduce quantitatively in the whole composition range even for the most popular atomistic force fields. In mixtures of OPLS-AA methanol and TIP4P-Ew or SPCE water, results for the enthalpy of mixing are very similar to ours, having the minimum at $\chi_{MeOH} \approx 0.55$ with values of ΔH_{mix} that are 35% and 14% lower than the experimental value.[64]

In Figure 2 (Right) we show the experimental surface tension as a function of composition together with the results from simulations obtained with our model and with atomistic force fields that include partial charges. Our results show a less steeped change in σ^{lv} as χ_{Am} increases when compared to the experimental curve. In this case the experimental data is adjusted better with the other models based on TraPPE-UA or OPLSS-AA for methanol and on TIP4P for water.[65]

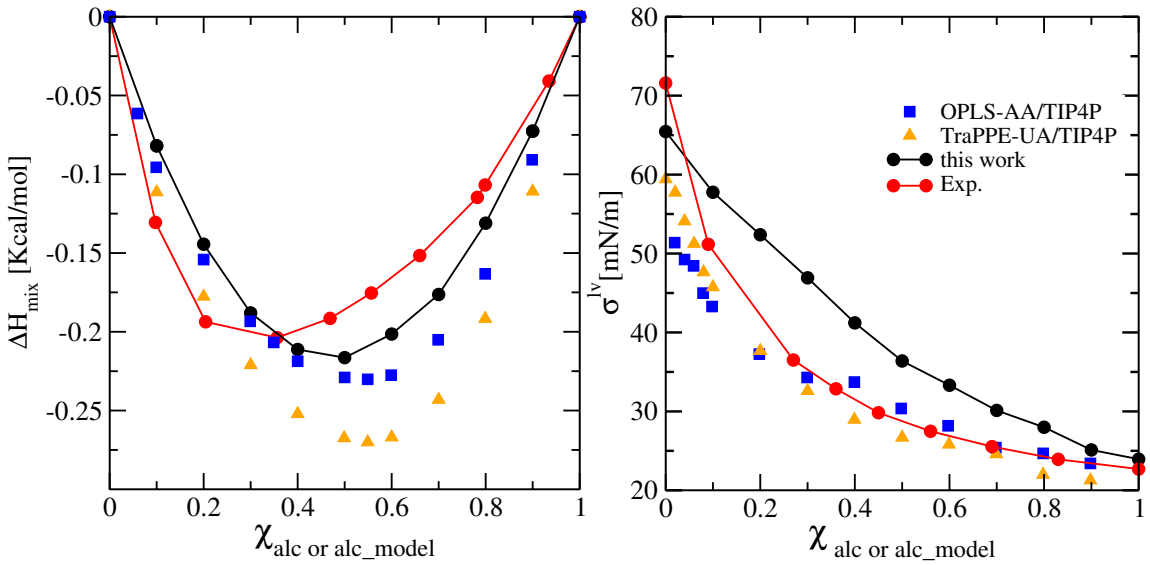

Figure 2: Enthalpy of mixing (Left) and surface tension (Right) as a function of the alcohol molar fraction for the aqueous solution. Black dots line: results from this work. Red dots line: experimental data for methanol-water.[62,63] Orange triangles: simulations results for methanol-water mixtures described with TraPPE-U and TIP4P.[65] Blue squares: simulations results for methanol-water mixtures described with OPLS-AA and TIP4P.[65]

We make the point that we explicitly refer to our amphiphilic model molecule as Am, instead of methanol. It in fact reproduces some thermodynamics properties of methanol with an accuracy comparable with atomistic models, such as the heat of vaporization and surface tension. It also performs satisfactorily for mixtures with mW water molecules by reproducing the surface tension of the solutions and the excess heat of mixing. For the latter, it outperforms some of the most common atomistic models. The radial distribution functions associated with the Am-mW system were not included as a figure of merit for our parametrization. Overall, it provides a good description of many of the thermodynamic properties most relevant in the context of this study, at the expense of an overestimation of the density of pure methanol and its mixtures. Since our objective is the verification of the thermodynamic relations derived in sections III.A and III.B with an emphasis on water-alcohol solutions, the present coarse-grained model serves our purpose of capturing the generic features of alcohols while allowing for massive scale simulations that would be unfeasible with an atomistic method.

III.D Structural properties of the confined solutions

In this section, we describe the nature of Am-mW mixtures of several compositions confined in pores of radii 15 and 25 Å. Figure 3 presents the equilibrium molar fraction profile χ_{Am} and χ_{mW} along the pore axis, for global compositions χ°_{Am}=0.1, 0.2, 0.3, 0.4 and 0.5. These profiles quantify the equilibrium concentrations of Am and mW inside the pore, at the external surfaces of the pore block, and in the bulk reservoirs. In the pore region, they reflect an enrichment of Am and a concomitant mW depletion, a trend seen for the whole range of concentrations studied. Conversely, in the bulk region, the opposite process takes place, leading to a χ_{mW} increase linked to the reduction of χ_{Am}. On the other hand, prominent peaks for χ_{Am} characterize the external region of the pore block (at z=90 and 190 Å), indicating an accumulation of Am on both surfaces. Peaks corresponding to mW are slightly displaced further from both block surfaces as a consequence of layering next to the Am shell.

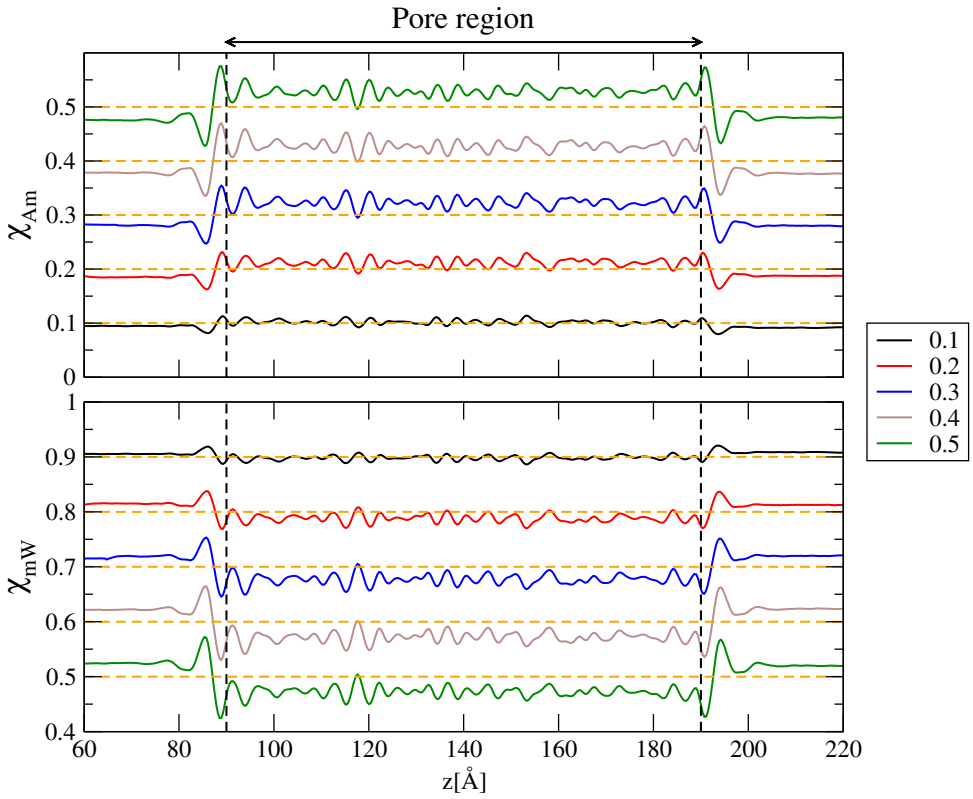

Figure 3: Molar fraction of Am molecules (top panel) and mW particles (bottom panel) for global molar fractions χ°_{Am}= 0.1, 0.2, 0.3, 0.4 and 0.5, along the pore axis z. The vertical black dashed lines indicates the beginning and end of the pore (z=90 and 190 Å). The horizontal dashed orange lines mark the global molar fraction for each case.

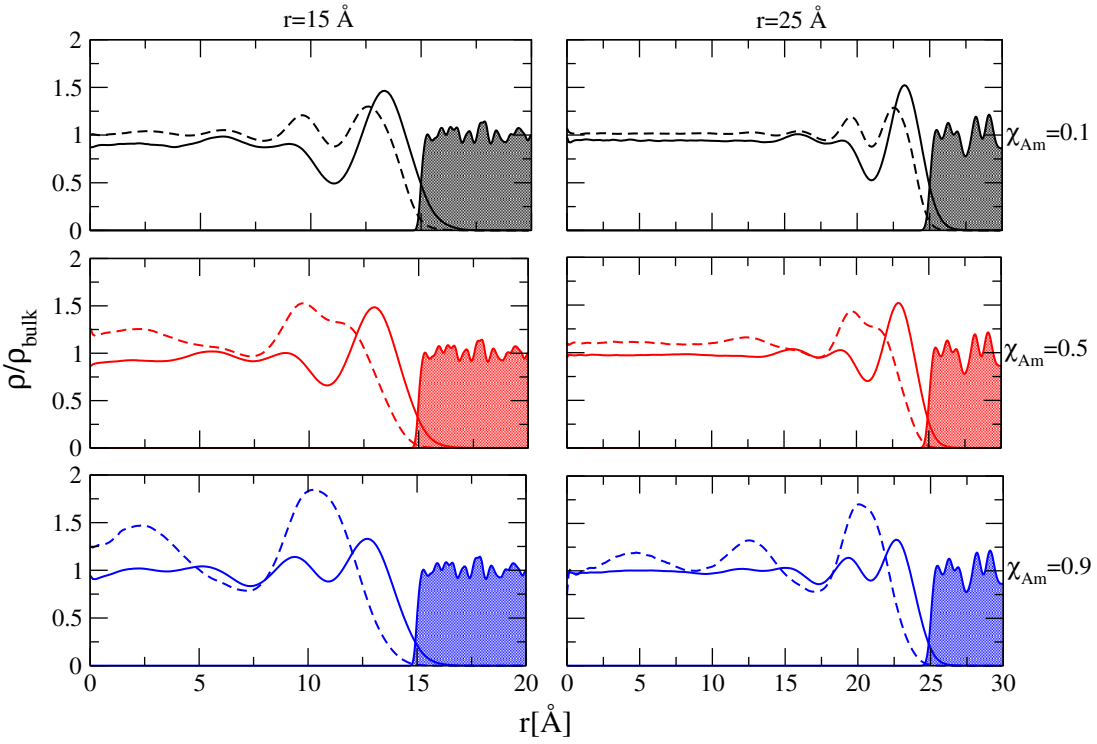

Figure 4: Radial density profiles normalized by the bulk density, for different global compositions χ°_{Am}=0.1 (top row black), 0.5 (middle row red) and 0.9 (lower row blue), for the pores with radius 15 (left column) and 25 Å (right column); r = 0 corresponds to the center of the pore. The solid and dashed lines are the Am and mW densities, respectively. The shaded areas correspond to the wall density.

Inside the pore, both substances are highly structured. The profiles $\chi_i(z)$ within this region given in Figure 3 are averaged on the radial coordinate, but the distribution along this coordinate is not homogeneous. Figure 4 depicts the radial density profiles for mW and Am at different molar fractions for the two pores of different radii, revealing the structuring originating from the interaction with the wall and the confinement. A pronounced density maximum of Am molecules (solid lines in Figure 4) appears near the pore wall surfaces, indicating that Am molecules form a compact layer near the solid surface in all cases. The Am density profiles become smoother towards the pore center, where they turn practically structureless ($\rho^{pore}_{Am} \sim \rho^{bulk}_{Am}$), which is more evident in the largest pore (r_p=25 Å, right panels

in Figure 4). For the mW particles, two density maxima appear, with one of them significantly overlapping with the Am density maximum when χ_{Am}=0.1 (top panel of Figure 4). As the alcohol concentration increases, the mW density maxima tend to merge and move away from the Am maximum (middle and bottom panels in Figure 4). This reflects the preferential adsorption of the Am molecules on the pore walls, where the increase in the global χ°_{Am} leads to higher surface coverages, expelling the mW particles that accumulate in a second sub-layer further from the wall.

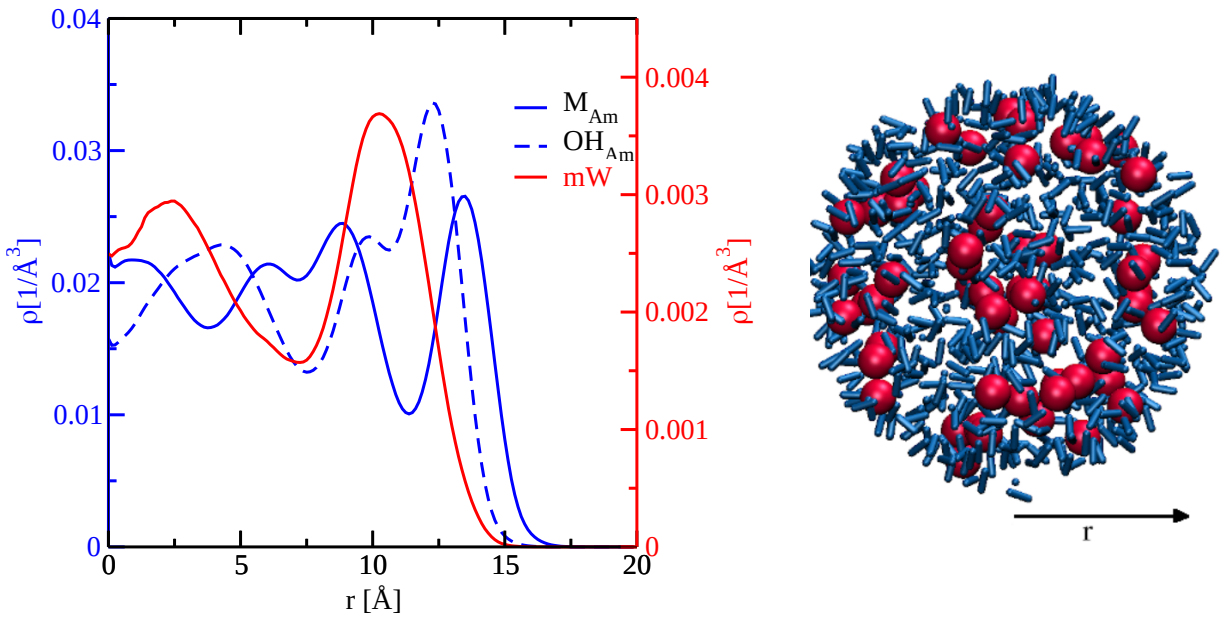

Figure 5: Left: number density profile as a function of the radial coordinate, for a mixture with χ°_{Am}=0.9 in a pore of radius 15 Å. The red line depicts the mW water profile, referenced on the right axis with same color. The blue continuous and dashed lines correspond to the hydrophobic and hydrophilic particles of the alcohol, M and OH respectively, both referenced on the left axis of same color. Right: structure of the solution inside the pore, extracted from the MD trajectory. Water (mW) and alcohol (Am) are displayed with red spheres and blue rods respectively.

In particular, for χ°_{Am}=0.9, the alternated Am/mW layer structure is more marked. This is illustrated in Figure 5. On the left panel we break down the density profile of the Am molecule in its constituents particles, the hydrophobic and hydrophilic parts (M and OH), represented with blue and dashed blue lines respectively. In the same graph we plot the density profile for mW water in red. A region rich in water localized at $\sim$ 10 Å is enclosed

between alcohol layers. The most external of the latter, extending from $\sim$ 10 to 14 Å, lies with the hydrophobic part facing the pore wall (blue line peak between 12.5 and 16 Å). A typical configuration at this composition is shown on the right panel, where the distribution of the particles matches the average density profiles. Overall, this suggests a mild segregation between mW water and Am alcohol at a global composition χ°_{Am}=0.9.

III.E The partition of the confined solution

The partition coefficient S, defined by the molar fractions (first quotient on the right in Eq.1), allows for the quantification of the separation ability of the pores. As already mentioned in the Methodology section, the adsorbed phase is not unequivocally defined neither in experiments nor in simulations. In both cases, it depends on an underlying model establishing the pore surface and volume, quantities that exhibit some degree of arbitrariness even in the simulations. Here we calculate the compositions, and therefore S, by averaging the molar fraction profile inside the pore (Figure 3).

The partition coefficient is presented in Figure 6 for pores of two different radii as a function of $\chi_{Am;ads}$. In Eq. 1 we take components A and B to represent the alcohol (Am) and water (mW) respectively, in which case $S > 1$ implies an enrichment of Am inside the pore linked to a concomitant increase of mW in the reservoirs. Two aspects are evident from a preliminary inspection of Figure 6. First, the pore with radius 15 Å shows a higher separation ability for the whole range of compositions, reflecting the dependence of the separative properties on the area/volume ratio. This dependence of S with respect to pore radius will be specifically explored later in this section.

Inside the pore, the volume of the first solvation shell represents a considerable fraction of the entire inner space, particularly for the pore of 15 Å. Hence, the accumulation of one of the species at the solid-liquid interface has in the smallest pore a strong impact on $\chi_{Am;ads}$, which becomes significantly higher than $\chi_{Am;blk}$. This is the fundamental reason for the partition.

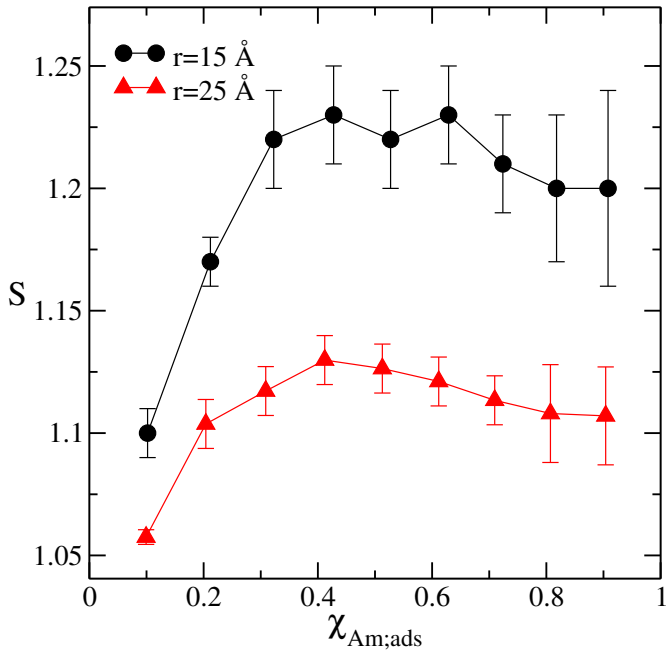

Figure 6: Partition coefficients as a function of the molar fraction of alcohol inside the pore. Black dots and red triangles correspond to pore radii of 15 and 25 Å respectively. Lines are just guidance for the eye.

Figure 6 shows that at low concentrations of alcohol the value of the partition coefficient is highly dependent on the composition of the mixture. For compositions $\chi_{Am;ads}$ above ~ 0.4 this trend changes and S becomes apparently constant, within the uncertainty of our simulations. In principle it can be expected that the partition coefficient is not invariant with the composition of the mixture, as it is computed in terms of molar fractions, not being a truly thermodynamic constant. However, Eq. 4 suggests that the partition constant will neither be invariant with respect to composition, since it depends on the product $\sigma^{lv}\cos(\theta)$ which in turn is determined by the concentration.

This behaviour has been loosely discussed in the literature in connection with molecular simulations. Kommu *et al.*[31] computed the partition coefficients of ethanol-water mixtures in carbon and hexagonal boron nitride plates separated by 13 Å as a function of the ethanol mole fraction, finding, similarly to the behavior reported above, a significant change in S at low concentration that tended to an asymptotic value as the molar fraction of ethanol increased. Bai *et al.*[59] calculated selectivity coefficient for methanol/water and ethanol/water mixtures

in zeolites using Gibbs Ensemble Monte Carlo simulations, showing also this same trend. However, no further analysis or interpretation were developed from these observations.

An explanation for the composition trend in S can be found investigating the two limits defined in section III.A (see Eqs. 5 and 6). In what follows we change the magnitude of the interaction between water and the surface, to produce different contact angles in our simulations. In Figure 8 the results obtained for S (as an estimate for K) with these different interactions are plotted as a function of $\sigma^{*;lv}_{Am} cos(\theta^*_{Am}) - \sigma^{*;lv}_{mW} cos(\theta^*_{mW})$ for two global compositions of the alcohol: 0.1 and 0.9.

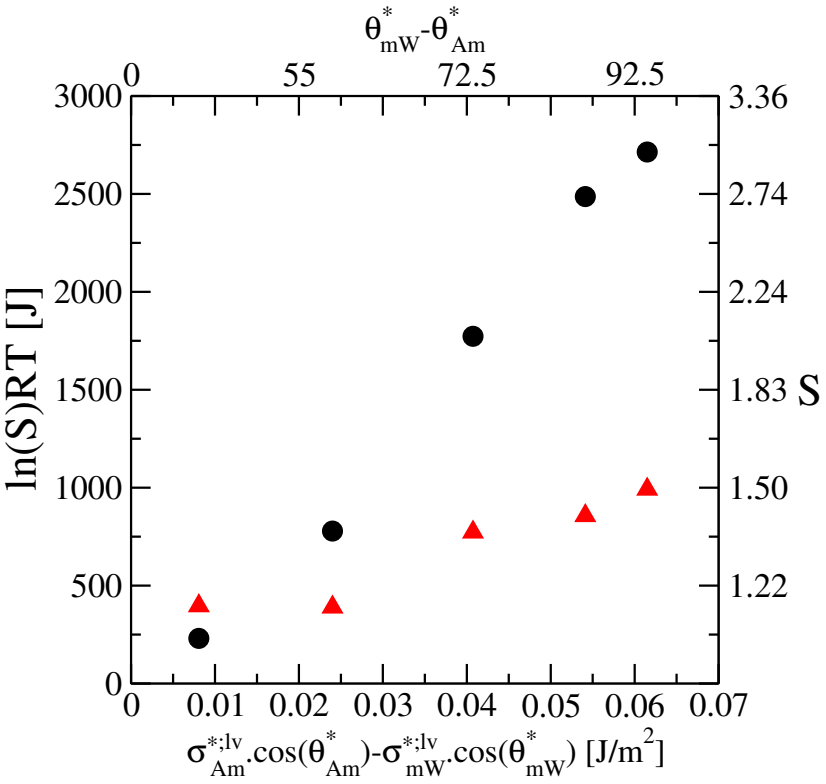

Figure 7: Partition coefficient as a function of the affinity of the solution for the pore surface (only the mW contact angle is varied). The affinity is expressed in terms of the contact angle. The lower x and the left y axes shows the scale relevant for the partition phenomena (see main text). The upper and right axes serves as a reference for the difference in contact angles and the value of the partition coefficient respectively. Results are shown for the partition coefficient at global compositions χ°_{Am}=0.1 (Black) and χ°_{Am}=0.9 (Red).

As can be seen, a rise in the difference between the contact angles of the pure substances effectively translates into a higher value of S. Moreover, according to the limiting

expressions corresponding to infinite dilution and pure alcohol (Eqs. 5 and 6), the slope in Figure 8 should be proportional to the molar surface area of the minority component. This is consistent with our results, showing a slope for χ°_{Am}=0.1 which is nearly twice the slope corresponding to χ°_{Am}=0.9. In particular, we estimated the molecular surface area of the components at different compositions employing the Voronoi tessellation methodology (utilizing the Voro++ code,[66] available within the LAMMPS distribution). The molecular surfaces areas computed for pure Am and mW are 23 and 13 Å^2 per molecule respectively, so that the surface area of Am approximately doubles that of mW, in notable agreement with the slopes of Figure 8. Our results for the pure systems are also in line with the experimental data obtained from gas adsorption isotherms,[53] reporting values of 22 and 13 Å^2 per molecule for methanol and water respectively. The fact that our Voronoi tessellation data agrees within 5% with the experimental results is surprising given that none of the models has been parameterized taking into account this property. Nevertheless, the molecular surface areas show a clear dependency on the composition of the mixture, varying 22% for Am (to 28 Å^2 at $\chi_{Am;ads}$=0.096) and -60% for mW (to 5.5 Å^2 at $\chi_{mW;ads}$=0.11), which is in conflict with one of the main hypothesis behind the model, assuming constant surface areas.

In any case, even when we are analyzing the behaviour of S, and not K, with the composition of the mixture and affinity to the surface, and in spite of the fact that the hypothesis of constant molar surface area does not seem to hold, the relationship between S and $\sigma^{*;lv}_{Am} cos(\theta^{*}_{Am}) - \sigma^{*;lv}_{mW} cos(\theta^{*}_{mW})$ results in a good semi-quantitative guide to the partition capabilities of a certain material.

Eq. 12 provides a relation between the partition constant and pore radius. To examine the validity of this result, we conducted several simulations for different pore radii ranging from 5 to 30 Å, for a global composition $\chi^{\circ}_{Am} = 0.5$. The affinity of the pore for the components is kept constant, with contact angles $\theta^{*}_{mW} = 80^{\circ}$ and $\theta^{*}_{Am} = 36^{\circ}$. We assume that the partition constant (K) is well represented by the partition coefficient (S). Figure 8 presents, in black circles, the logarithm of S resulting from the simulations, versus the

inverse of the pore radius. In the same Figure, the prediction for $\ln(K)$ obtained directly from equation 12 is depicted with red up triangles. The inset shows the full range of radii explored, including the data for the smallest pore with r_{pore}= 5 Å.

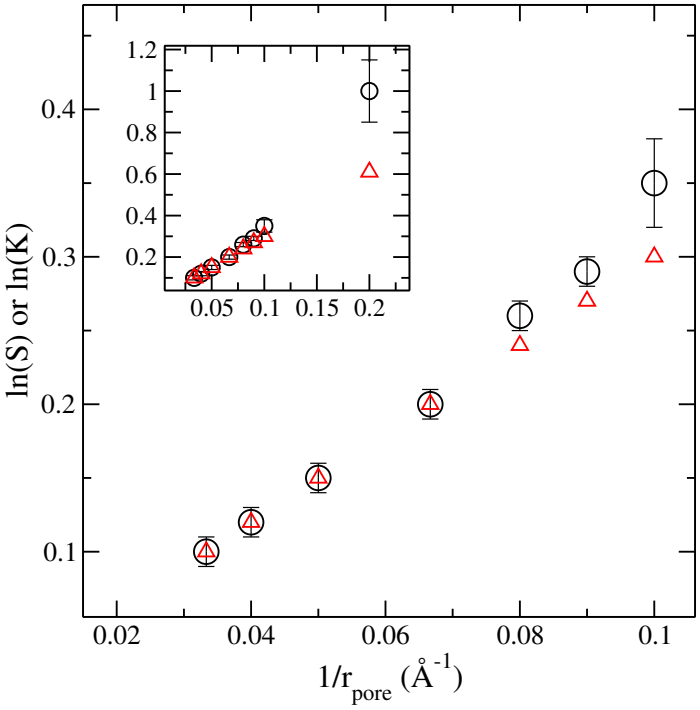

Figure 8: Natural logarithm form of the partition coefficient ($\ln(S)$) as a function of the inverse radius ($1/r_{pore}$). Results corresponding to the simulations (black circles) and to Eq. 11 (red triangles) are displayed for a global molar fraction of Am equal to 0.5.

As can be seen from the graph, the agreement between the simulations and the prediction of K for pores as small as 14 Å radius (or $1/r_{pore} \geq 0.07$ Å^{-1}) is remarkable. The agreement is very good despite the fact that we consider S and not K, which suggests that the excess effects in the chemical potential might compensate between the species involved in the partition, at least for a composition near 0.5. The deviation observed for pores of small radii is not surprising and have been seen for other kinds of equilibrium also describable by Kelvin-type equations. For example, in previous work we showed, using molecular simulations, that the vapor pressure dependence of the radius of water droplets follows the Kelvin equation for clusters greater than 1 nm diameter.[40] Recently, AFM experiments by Yang *et al.*[67] tested the validity of the Kelvin equation for water under 2D confinement at the molecular scale.

These authors showed that the vapor pressure of the system could be predicted by the thermodynamic equation down to channel heights of 2 nm for both hydrophilic and hydrophobic walls. Work by Wang and collaborators[68] addressing the vapor-liquid equilibrium for confined propane compared predictions of the Kelvin equation and other equations of state with results from classical density functional theory (DFT) and available experimental data. This study indicated that DFT can reasonably approximate experimental data in pores of 10 nm width, and that the equations derived from classical thermodynamics and DFT agree for pore dimensions greater than 10 nm, but diverge below this critical size.

There is no definite explanation of why this type of Kelvin equation based on macroscopic arguments can describe equilibrium at such small scales. The difference in the breaking point for the data reported for propane, an order of magnitude above compared to that arising from our studies on aqueous clusters or from AFM experiments for water, suggests that the size of the confinement relative to that of the confined molecules plays a key role in predicting the range of applicability of the Kelvin equation. To explore this hypothesis in the present system, Figure 9 illustrates the density profiles of Am in the pores for radii 30, 15, 10 and 5 Å. The profiles are shown shifted by the radius of the pore (plotted as $r_{pore} - r$), to convey the relative magnitude of the perturbation compared to the dimension of the pore. It can be appreciated that the perturbation in the density caused by the wall is almost independent of the pore radius. More specifically, the major difference is that whereas pores smaller than 15 Å can just accommodate part of the perturbation, bigger pores contain it fully, plus a region where the density of the mixture is homogeneous and practically equal to that of bulk. For this system the deviation from the Kelvin equation is observed when the inhomogeneity in the density extends through the full volume of the pore, excluding the presence of bulk-like solution.

In previous work, we argued that the Kelvin equation could be expected to be accurate at the nanoscale provided that the major hypothesis underlying its derivation (e.g. homogeneous phases and well defined interfaces) are satisfied, not in an instantaneous sense, but in

terms of time-averages of the density profiles.[40] For those pores larger than 15 Å the fluid density can be in fact considered to be constant and approximately equal to the bulk value, which is not the case for smaller radii. Besides, the characteristic times associated with the degrees of freedom of the confined species will be shorter for smaller molecules, and then the profiles for water structures inside a tiny nanpore are likely to become homogeneous in shorter periods compared to propane.

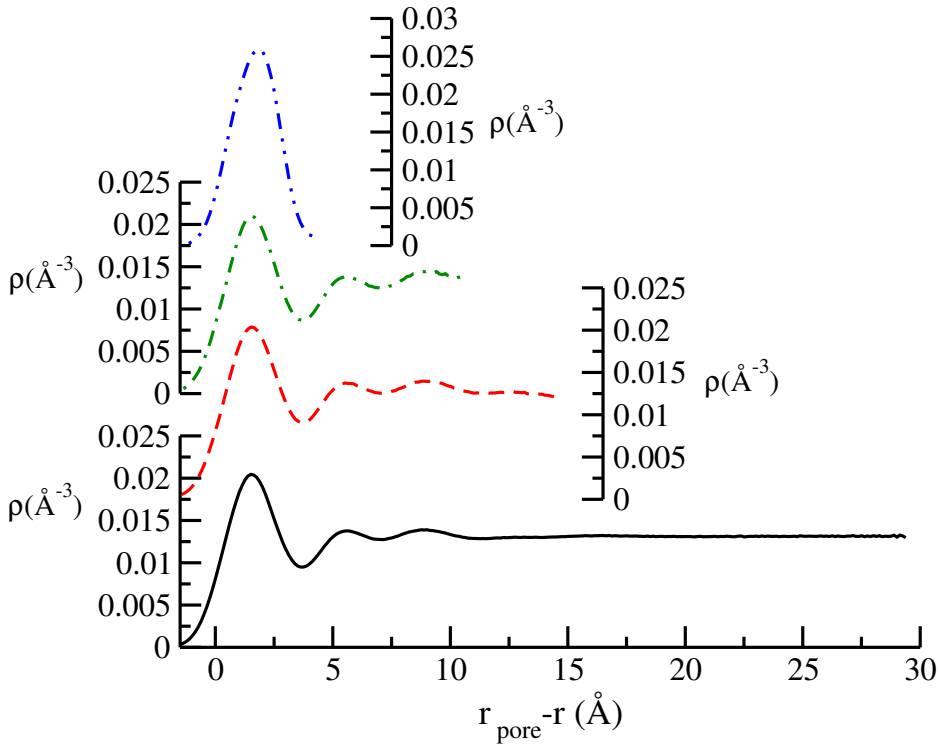

Figure 9: Shifted radial density profiles of Am inside the pore of different radius. Black-continues 30 Å, Red-breake 15 Å, Green-break-dotted 10 Å, Blue-break-doubled dotted 5Å

IV. Summary and conclusions

In this work we have performed molecular simulations to scrutinize different formalisms aiming to describe the partition phenomenon in confined systems. As our test model we studied mixtures of a generic alcohol (or the amphiphilic molecule Am, exhibiting some of the properties of methanol) and water (described with the mW potential) confined in a

cylindrical nanopore. We characterized the segregation ability of the pore in terms of the partition coefficient S, which turned out to be highly dependent on three key factors: the composition of the mixture, the interaction of its components with the pore surface, and the radius of the pore. All three variables were rationalized in terms of an appropriate theory.

The use of a coarse grained model allowed us to perform long timescale simulations (up to five replicas for 200 ns) on systems containing more than 20000 molecules, which is far above the sampling commonly achievable for this type of systems with atomistic potentials. The Am molecule reproduces the enthalpy of vaporization and surface tension of pure methanol with a discrepancy of 10 % with respect to the experimental data. For water-alcohol mixtures it reproduces the dependence of the excess enthalpy of mixing with the molar fraction of the solution with the minimum displaced in around 0.2 units of molar fraction with respect to the experimental data and a value 10 % lower, performing better than the most used all-atom potentials such as TraPPE-UA or OPLSS-AA. The liquid-vapor surface tension for the mixture was captured with an accuracy comparable to that provided by the atomistic models. In return, the density of the pure liquid and its solutions was significantly overestimated with respect to that corresponding to methanol.

To explain the composition dependence of S, we elaborated on the multilayer adsorption model presented by Gritti *et al.*[53] This theory predicts that neither the partition coefficient (S) nor the partition constant (K) should be independent of the composition. By combining this model with the Young equation, we concluded that, for binary mixtures, the difference $\sigma_1^{*;lv} cos(\theta_1^*) - \sigma_2^{*;lv} cos(\theta_2^*)$ can predict the separation capability of a certain material for a given solution. We tested this relation for the regimes of high and low concentration for our Am-mW system varying the interaction with the pore. The resulting trend agrees with the theory in a semi-quantitative manner. The relevance of this result resides in its potential application as a practical estimator of the separative efficiency. The liquid-vapor surface tension and contact angles are properties readily accessible from both experiments and simulations, and therefore the availability of an expression that estimates the partition coefficient in terms of

these variables can be extremely useful.

We introduced a model based on the Kelvin equation that relates the partition coefficient with the radius of the pore. This model assumes that the components of the solution do not interact between them. Nevertheless, it is able to reproduce the behaviour of an equimolar mixture of water and alcohol confined in pores of radius larger than 15 Å and of a mildly hydrophobic surface ($\theta_{mW} \approx 80°$). The fact that the Kelvin equation fails at smaller diameters can be understood in terms of the relation between the confining media and the confined species, following the same line of thought of previous works.[40,67,68] Specifically, we found that the confining matrix generates a perturbation on the radial density profile of the components of the solution that propagates to the center of the pore. When the inhomogeneity extends through most of the pore, the proposed model based on the Kelvin equation fails. The success of this model for this particular case should encourage further theoretical developments, su as the incorporation of more specific descriptors for the mixtures.

Acknowledgement

This study has been funded by grants of the Agencia Nacional de Promoción Científica y Tecnológica de Argentina (PICT 2016-3167) and of CONICET (PIP 11220200103117CO). We thank computation time provided by the high performance computing facilities CECAR and TUPAC. AHC acknowledges CONICET for a postdoctoral fellowship.

References

(1) Krueger, A. *Carbon materials and nanotechnology*; Wiley-VCH: Weinheim, Germany, 2010.

(2) Benzigar, M. R.; Talapaneni, S. N.; Joseph, S.; Ramadass, K.; Singh, G.; Scaranto, J.; Ravon, U.; Al-Bahily, K.; Vinu, A. Recent advances in functionalized micro and meso-

porous carbon materials: synthesis and applications. *Chem. Soc. Rev.* **2018**, *47*, 2680–2721.

(3) Emparan-Legaspi, M. J.; Gonzalez, J.; Gonzalez-Carrillo, G.; Ceballos-Magaña, S. G.; Canales-Vazquez, J.; Aguayo-Villarreal, I. A.; Muñiz-Valencia, R. Dynamic adsorption separation of benzene/cyclohexane mixtures on micro-mesoporous silica SBA-2. *Microporous Mesoporous Mater* **2020**, *294*, 109942.

(4) Florek, J.; Giret, S.; Juère, E.; Larivière, D.; Kleitz, F. Functionalization of mesoporous materials for lanthanide and actinide extraction. *Dalton Trans.* **2016**, *45*, 14832–14854.

(5) Olajire, A. A. Synthesis of bare and functionalized porous adsorbent materials for CO capture. *Greenhouse Gas Sci Technol* **2017**, *7*, 399–459.

(6) Zheng, M.; Jagota, A.; Semke, E. D.; Diner, B. A.; Mclean, R. S.; Lustig, S. R.; Richardson, R. E.; Tassi, N. G. DNA-assisted dispersion and separation of carbon nanotubes. *Nature Mater* **2003**, *2*, 338–342.

(7) Kim, W.; Nair, S. Membranes from nanoporous 1D and 2D materials: A review of opportunities, developments, and challenges. *Chem. Eng. Sci.* **2013**, *104*, 908–924.

(8) Musarurwa, H.; Tawanda Tavengwa, N. Recent progress in the application of pH-responsive polymers in separation science. *Microchem. J.* **2022**, *179*, 107503.

(9) Zhang, W.; Aguila, B.; Ma, S. Potential applications of functional porous organic polymer materials. *J. Mater. Chem. A* **2017**, *5*, 8795 – 8824.

(10) Everett, D. H. Thermodynamics of adsorption from solution. Part 1.—Perfect systems. *Trans. Faraday Soc.* **1964**, *60*, 1803–1813.

(11) Everett, D. H. Reporting data on adsorption from solution at the solid/solution interface (Recommendations 1986). *Pure Appl. Chem.* **1986**, *58*, 967–984.

(12) Kazakevich, Y. High-performance liquid chromatography retention mechanisms and their mathematical descriptions. *J. Chromatogr. A* **2006**, *1126*, 232–243, The Role of Theory in Chromatography.

(13) Faucher, S. et al. Critical Knowledge Gaps in Mass Transport through Single-Digit Nanopores: A Review and Perspective. *J. Phys. Chem. C* **2019**, *123*, 21309–21326.

(14) Lei, W.; Portehault, D.; Liu, D.; Qin, S.; Chen, Y. Porous boron nitride nanosheets for effective water cleaning. *Nat Commun* **2013**, *4*, 1777.

(15) Liu, G.; Shen, J.; Ji, Y.; Liu, Q.; Liu, G.; Yang, J.; Jin, W. Two-dimensional Ti_2CT_x MXene membranes with integrated and ordered nanochannels for efficient solvent dehydration. *J. Mater. Chem. A* **2019**, *7*, 12095–12104.

(16) El-Roz, M.; Bazin, P.; Čelič, T. B.; Logar, N. Z.; Thibault-Starzyk, F. Pore Occupancy Changes Water/Ethanol Separation in a Metal–Organic Framework—Quantitative Map of Coadsorption by IR. *J. Phys. Chem. C* **2015**, *119*, 22570–22576.

(17) Muthulakshmi, T.; Dutta, D.; Maheshwari, P.; Pujari, P. K. Evidence for confinement induced phase separation in ethanol–water mixture: a positron annihilation study. *J. Phys.: Condens. Matter* **2018**, *30*, 025001.

(18) Boffa, V.; Etmimi, H.; Mallon, P.; Tao, H.; Magnacca, G.; Yue, Y. Carbon-based building blocks for alcohol dehydration membranes with disorder-enhanced water permeability. *Carbon* **2017**, *118*, 458–466.

(19) Guan, K.; Liang, F.; Zhu, H.; Zhao, J.; Jin, W. Incorporating Graphene Oxide into Alginate Polymer with a Cationic Intermediate To Strengthen Membrane Dehydration Performance. *ACS Appl. Mater. Interfaces* **2018**, *10*, 13903–13913.

(20) Gelb, L. D.; Gubbins, K. E.; Radhakrishnan, R.; Sliwinska-Bartkowiak, M. Phase separation in confined systems. *Rep. Prog. Phys.* **2000**, *63*, 727–727.

(21) Binder, K.; Puri, S.; Das, S. K.; Horbach, J. Phase Separation in Confined Geometries. *J Stat Phys* **2010**, *138*, 51–84.

(22) Bampoulis, P.; Witteveen, J. P.; Kooij, E. S.; Lohse, D.; Poelsema, B.; Zandvliet, H. J. W. Structure and Dynamics of Confined Alcohol–Water Mixtures. *ACS Nano* **2016**, *10*, 6762–6768.

(23) Hamid, A. R. A.; Mhanna, R.; Lefort, R.; Ghoufi, A.; Alba-Simionesco, C.; Frick, B.; Morineau, D. Microphase Separation of Binary Liquids Confined in Cylindrical Pores. *J. Phys. Chem. C* **2016**, *120*, 9245–9252.

(24) Videla, P. E.; Sala, J.; Martí, J.; Guàrdia, E.; Laria, D. Aqueous electrolytes confined within functionalized silica nanopores. *J. Chem. Phys.* **2011**, *135*, 104503.

(25) Rodriguez, J.; Elola, M. D.; Laria, D. Confined Polar Mixtures within Cylindrical Nanocavities. *J. Phys. Chem. B* **2010**, *114*, 7900–7908, PMID: 20499844.

(26) Rodriguez, J.; Elola, M. D.; Laria, D. Polar Mixtures under Nanoconfinement. *J. Phys. Chem. B* **2009**, *113*, 12744–12749, PMID: 19757844.

(27) Zhao, W.-H.; Shang, B.; Du, S.-P.; Yuan, L.-F.; Yang, J.; Zeng, X. C. Highly selective adsorption of methanol in carbon nanotubes immersed in methanol-water solution. *J. Chem. Phys.* **2012**, *137*, 034501.

(28) Tian, X.; Yang, Z.; Zhou, B.; Xiu, P.; Tu, Y. Alcohol-induced drying of carbon nanotubes and its implications for alcohol/water separation: A molecular dynamics study. *J. Chem. Phys.* **2013**, *138*, 204711.

(29) Phan, A.; Cole, D. R.; Striolo, A. Preferential Adsorption from Liquid Water–Ethanol Mixtures in Alumina Pores. *Langmuir* **2014**, *30*, 8066–8077.

(30) Zhao, M.; Yang, X. Segregation Structures and Miscellaneous Diffusions for

Ethanol/Water Mixtures in Graphene-Based Nanoscale Pores. *J. Phys. Chem. C* **2015**, *119*, 21664–21673.

(31) Kommu, A.; Singh, J. K. Separation of Ethanol and Water Using Graphene and Hexagonal Boron Nitride Slit Pores: A Molecular Dynamics Study. *J. Phys. Chem. C* **2017**, *121*, 7867–7880.

(32) Prslja, P.; Lomba, E.; Gómez-Álvarez, P.; Urbič, T.; Noya, E. G. Adsorption of water, methanol, and their mixtures in slit graphite pores. *J. Chem. Phys.* **2019**, *150*, 024705.

(33) Qin, Y.; Zhao, N.; Zhu, Y.; Zhang, Y.; Gao, Q.; Dai, Z.; You, Y.; Lu, X. Molecular insights into the microstructure of ethanol/water binary mixtures confined within typical 2D nanoslits: The role of the adsorbed layers induced by different solid surfaces. *Fluid Phase Equilibria* **2020**, *509*, 112452.

(34) Molinero, V.; Moore, E. B. Water Modeled As an Intermediate Element between Carbon and Silicon. *J. Phys. Chem. B* **2009**, *113*, 4008–4016.

(35) Stillinger, F. H.; Weber, T. A. Computer simulation of local order in condensed phases of silicon. *Phys. Rev. B* **1985**, *31*, 5262–5271.

(36) Factorovich, M. H.; Solveyra, E. G.; Molinero, V.; Scherlis, D. A. Sorption Isotherms of Water in Nanopores: Relationship Between Hydropohobicity, Adsorption Pressure, and Hysteresis. *J. Phys. Chem. C* **2014**, *118*, 16290–16300.

(37) Lupi, L.; Kastelowitz, N.; Molinero, V. Vapor deposition of water on graphitic surfaces: Formation of amorphous ice, bilayer ice, ice I, and liquid water. *J. Chem. Phys* **2014**, *141*, 18C508.

(38) Moore, E. B.; Molinero, V. Structural transformation in supercooled water controls the crystallization rate of ice. *Nature* **2011**, *479*, 506–508.

(39) Moore, E. B.; Allen, J. T.; Molinero, V. Liquid-Ice Coexistence below the Melting Temperature for Water Confined in Hydrophilic and Hydrophobic Nanopores. *J. Phys. Chem. C* **2012**, *116*, 7507–7514.

(40) Factorovich, M. H.; Molinero, V.; Scherlis, D. A. Vapor Pressure of Water Nanodroplets. *J. Am. Chem. Soc.* **2014**, *136*, 4508–4514.

(41) de la Llave, E.; Molinero, V.; Scherlis, D. A. Role of Confinement and Surface Affinity on Filling Mechanisms and Sorption Hysteresis of Water in Nanopores. *J. Phys. Chem. C* **2012**, *116*, 1833–1840.

(42) Lupi, L.; Hudait, A.; Molinero, V. Heterogeneous Nucleation of Ice on Carbon Surfaces. *J. Am. Chem. Soc.* **2014**, *136*, 3156–3164.

(43) Xu, L.; Molinero, V. Liquid-Vapor Oscillations of Water Nanoconfined between Hydrophobic Disks: Thermodynamics and Kinetics. *J. Phys. Chem. B* **2010**, *114*, 7320–7328.

(44) Jorgensen, W. L. Optimized intermolecular potential functions for liquid alcohols. *J. Phys. Chem.* **1986**, *90*, 1276–1284.

(45) Qiu, Y.; Odendahl, N.; Hudait, A.; Mason, R.; Bertram, A. K.; Paesani, F.; DeMott, P. J.; Molinero, V. Ice Nucleation Efficiency of Hydroxylated Organic Surfaces Is Controlled by Their Structural Fluctuations and Mismatch to Ice. *J. Am. Chem. Soc.* **2017**, *139*, 3052–3064.

(46) de la Llave, E.; Molinero, V.; Scherlis, D. A. Water filling of hydrophilic nanopores. *J. Chem. Phys* **2010**, *133*, 034513.

(47) Factorovich, M. H.; Molinero, V.; Scherlis, D. A. Hydrogen-Bond Heterogeneity Boosts Hydrophobicity of Solid Interfaces. *J. Am. Chem. Soc.* **2015**, *137*, 10618–10623.

(48) Giovambattista, N.; Debenedetti, P. G.; Rossky, P. J. Effect of Surface Polarity on Water Contact Angle and Interfacial Hydration Structure. *J. Phys. Chem. B* **2007**, *111*, 9581–9587.

(49) Hartwig, J.; Mann, J. A. Bubble point pressures of binary methanol/water mixtures in fine-mesh screens. *AIChE J.* **2014**, *60*, 730–739.

(50) Park, J.; Kang, Z.; Bender, G.; Ulsh, M.; Mauger, S. A. Roll-to-roll production of catalyst coated membranes for low-temperature electrolyzers. *J. Power Sources* **2020**, *479*, 228819.

(51) Parale, V.; Mahadik, D.; Mahadik, S.; Kavale, M.; Venkateswara Rao, A.; Wagh, P. Wettability study of surface modified silica aerogels with different silylating agents. *J. Sol-Gel Sci. Technol.* **2012**, *63*, 573–579.

(52) Plimpton, S. Fast Parallel Algorithms for Short-Range Molecular Dynamics. *J. Comput. Phys.* **1995**, *117*, 1–19.

(53) Gritti, F.; Guiochon, G. Thermodynamics of adsorption of binary aqueous organic liquid mixtures on a RPLC adsorbent. *J. Chromatogr. A* **2007**, *1155*, 85–99, 19th Annual International Ion Chromatography Symposium.

(54) Jantsch, E.; Koop, T. Cloud Activation via Formation of Water and Ice on Various Types of Porous Aerosol Particles. *ACS Earth Space Chem.* **2021**, *5*, 604–617.

(55) Shardt, N.; Elliott, J. A. W. Isobaric Vapor–Liquid Phase Diagrams for Multicomponent Systems with Nanoscale Radii of Curvature. *The Journal of Physical Chemistry B* **2018**, *122*, 2434–2447, PMID: 29442515.

(56) Rajput, V.; Ertekin, T. Thermodynamically-Consistent Modeling of Adsorption in Liquid-Rich Shales. **2014**, *All Days*, SPE-169589-MS.

(57) Adamson, T.; Adamson, A.; Gast, A. *Physical Chemistry of Surfaces*; A Wiley-Interscience publication; Wiley, 1997; Chapter 11, pp 408–410.

(58) Kipling, J. J.; Tester, D. A. 792. Adsorption from binary mixtures: determination of individual adsorption isotherms. *J. Chem. Soc.* **1952**, 4123–4133.

(59) Bai, P.; Tsapatsis, M.; Siepmann, J. I. Multicomponent Adsorption of Alcohols onto Silicalite-1 from Aqueous Solution: Isotherms, Structural Analysis, and Assessment of Ideal Adsorbed Solution Theory. *Langmuir* **2012**, *28*, 15566–15576.

(60) Caleman, C.; van Maaren, P. J.; Hong, M.; Hub, J. S.; Costa, L. T.; van der Spoel, D. Force Field Benchmark of Organic Liquids: Density, Enthalpy of Vaporization, Heat Capacities, Surface Tension, Isothermal Compressibility, Volumetric Expansion Coefficient, and Dielectric Constant. *J. Chem. Theory Comput.* **2012**, *8*, 61–74.

(61) Mikhail, S. Z.; Kimel, W. R. Densities and Viscosities of Methanol-Water Mixtures. *J. Chem. Eng. Data* **1961**, *6*, 533–537.

(62) Lama, R. F.; Lu, B. C. Excess Thermodynamic Properties of Aqueous Alcohol Solutions. *J. Chem. Eng. Data* **1965**, *10*, 216–219.

(63) Vazquez, G.; Alvarez, E.; Navaza, J. M. Surface Tension of Alcohol Water + Water from 20 to 50 .degree.C. *J. Chem. Eng. Data* **1995**, *40*, 611–614.

(64) Galicia-Andrés, E.; Dominguez, H.; Pusztai, L.; Pizio, O. Composition dependence of thermodynamic, dynamic and dielectric properties of water–methanol model mixtures. Molecular dynamics simulation results with the OPLS-AA model for methanol. *J. Mol. Liq.* **2015**, *212*, 70–78.

(65) Obeidat, A.; Abu-Ghazleh, H. The validity of the potential model in predicting the structural, dynamical, thermodynamic properties of the unary and binary mixture of water-alcohol: Methanol-water case. *AIP Adv.* **2018**, *8*, 065203.

(66) Rycroft, C. H. Voro++ original code. 2008; `https://math.lbl.gov/voro++/`.

(67) Yang, Q.; Sun, P.; Fumagalli, L.; Stebunov, Y.; Haigh, S.; Zhou, Z.; Grigorieva, I.; Wang, F.; Geim, A. Capillary condensation under atomic-scale confinement. *Nature* **2020**, *588*, 250–253.

(68) Wang, Y.; Shardt, N.; Lu, C.; Li, H.; Elliott, J. A.; Jin, Z. Validity of the Kelvin equation and the equation-of-state-with-capillary-pressure model for the phase behavior of a pure component under nanoconfinement. *Chem. Eng. Sci.* **2020**, *226*, 115839.

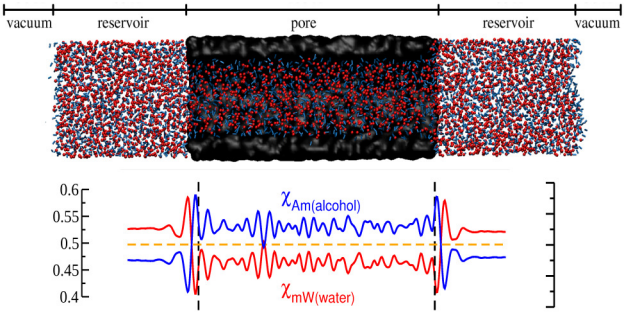
vacuum
reservoir
pore
reservoir
vacuum
0.6
0.55
0.5
0.45
0.4
χAm(alcohol)
χmW(water)

TOC Graphic